NMR identification of hydrophobic cavities with low water occupancies in protein structures using small gas molecules

Gottfried Otting[1], Edvards Liepinsh[1], Bertil Halle[2] and Urban Frey[3]

Magnetization transfer through dipole-dipole interactions (nuclear Overhauser effects, NOEs) between water protons and the protons lining two small hydrophobic cavities in hen egg-white lysozyme demonstrates the presence of water molecules with occupancies of ~10–50%. Similarly, NOEs were observed between the cavity protons and the protons of hydrogen, methane, ethylene or cyclopropane applied at 1–200 bar pressure. These gases can thus be used as general NMR indicators of empty or partially hydrated hydrophobic cavities in proteins. All gases reside in the cavities for longer than 1 ns in marked contrast to common belief that gas diffusion in proteins is not much slower than in water. Binding to otherwise empty cavities may be a major aspect of the anesthetic effect of small organic gas molecules.

Hydrophobic cavities in the interior of protein structures are usually found to be devoid of water molecules in X-ray crystallographic studies. NMR results indicate that such 'empty' space may be filled by disordered water molecules[1], but the results have been controversial[2–5]. Crystallographically empty cavities in protein structures have long been probed using xenon or cyclopropane[6–8]. Although xenon can be detected by NMR spectroscopy, the protons of small gas molecules offer much better sensitivity and the possibility to localize the gas molecules by intermolecular NOEs with the protein. Cyclopropane has a van der Waals volume comparable to that of xenon and smaller, differently shaped molecules are available that carry protons.

The present study of hen egg-white lysozyme (HEWL) in aqueous solution demonstrates that small hydrophobic cavities exist in wild-type HEWL which are partially filled with water. Earlier, we observed that methylene chloride not only binds to the substrate binding site C in the active site cleft of HEWL, but also penetrates into the protein interior[9]. Here we show that hydrogen, methane, ethylene and cyclopropane preferentially occupy the empty space of the hydrophobic cavities compared to stably hydrated sites. Thus, small organic gas molecules present sensitive and selective probes for the detection of empty hydrophobic cavities in proteins by NMR spectroscopy. Larger molecules bind with higher affinity, as long as they fit into the cavities. Clearly, empty or poorly hydrated hydrophobic cavities in proteins or formed between protein and lipid molecules in a membrane would represent high affinity binding sites for typical anesthetic compounds.

Hydrophobic cavities in HEWL

The Brookhaven protein data bank (PDB)[10] contains the coordinates of HEWL in several different crystal forms (PDB accession codes 4LYM[11], 1HEL[12], 1LZT[13], 2LZT[14]), under different pressures (2LYM[15], 3LYM[15]) and temperatures (5LYT[16], 6LYT[16]), of mutant variants (1HHL[17], 2IHL[18], 1LSN[19], 1LSM[19], 1HEM[20]), and of wild-type and mutant HEWL in co-crystals with ligands (1HEW[21], 1LSZ[22]). The hydrophobic core of the protein is completely conserved between all these structures and contains three hydrophobic cavities defined by the side chains of Leu 8, Met 12, Leu 17, Ile 55, Leu 56, Ile 88, Ser 91, Val 92 (cavity I); Trp 28, Ala 31, Leu 56, Met 105, Trp 108 (cavity II); and Leu 17, Tyr 20, Trp 28, Ala 95, Lys 96, Val 99 (cavity III) (Fig. 1). The water accessible volumes of the cavities are about 40, 11 and 13 Å^3 respectively. With a single exception, no hydration water molecules were reported in any of the three cavities. The exception is the structure 2LYM[15], where the water molecule W226 was placed near cavity I with an O–N distance of 2.1 Å to the nitrogen of Val 92, that is, at a distance much shorter than van der Waals or hydrogen bonding distance. Assuming that this water molecule was erroneously assigned, the combined X-ray data indicate that the hydrophobic cavities in HEWL are empty.

Cavity I provides sufficient space for two water molecules, but there is no possibility for hydrogen bonding with the cavity walls. The nearest polar atom is the amide proton of Val 92, which is just beyond van der Waals distance for cavity water. This amide proton is hydrogen bonded to the carbonyl oxygen of Ile 88 and is in an unfavourable orientation for hydrogen bonding with cavity water (Fig. 1*b*). Cavity II could accommodate a single water molecule, perhaps with a hydrogen bond to the aromatic side chain of Trp 108 (Fig. 1*c*). No hydrogen bonds can be formed in cavity III (Fig. 1*d*).

Our NMR experiments detected hydration water and gas molecules in cavities I and II, but not in cavity III. Cavity III is closest to the protein surface, separated from the bulk solvent by

[1]Karolinska Institute, Department of Medical Biochemistry and Biophysics, S-171 77 Stockholm, Sweden [2]Condensed Matter Magnetic Resonance Group, Department of Chemistry, Lund University, S-22100 Lund, Sweden [3]Université Lausanne, Institut de Chimie Minerale et Analytique, BCH, CH-1015 Lausanne, Switzerland

Correspondence should be addressed to G.O. *go@mfn.ki.se*

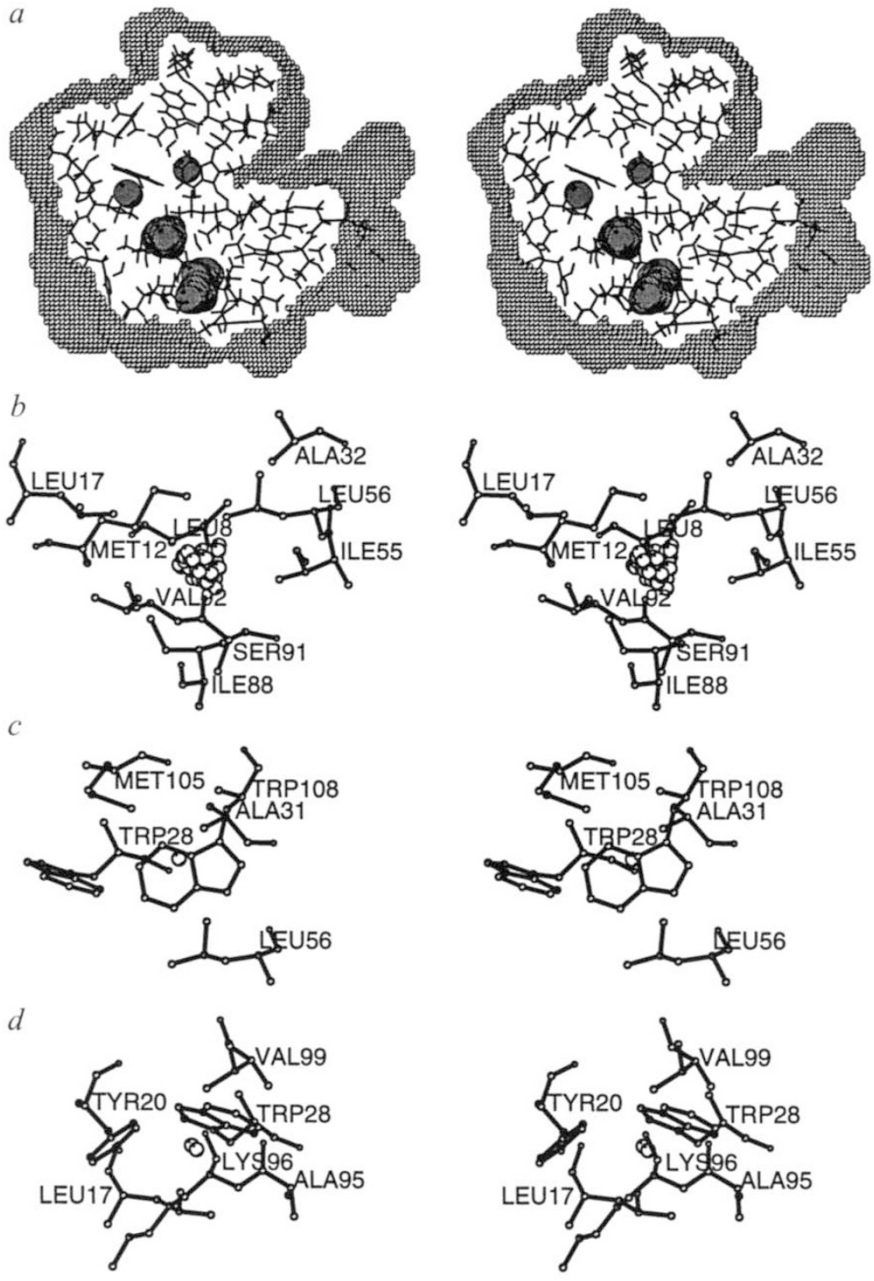

Fig. 1 Cavities in hen egg-white lysozyme (HEWL). *a*, Cross-section through the crystal structure[15] showing the protein in an all-atom representation. The protein surface is outlined by small spheres indicating the positions where water molecules of 1.4 Å radius could be placed at van der Waals distance from the protein atoms. The substrate binding cleft is at the north-east side of the surface representation. Spheres of 1.4 Å radius in the protein interior identify three hydrophobic cavities and one large cavity which contains the hydration water molecules W130, W131 and W180 in the crystal structure[15]. The cavities are from top to bottom: cavity II, cavity III, cavity I, and the hydrated cavity. *b–d*, Cavities I, II, and III, respectively, with their surrounding amino acid residues. Only heavy atoms are shown, with labels at the Cα atoms. Cavity coordinates, where water molecules of 1.4 Å radius could be placed without van der Waals violations with the surrounding protein atoms, are identified by spheres of 0.3 Å radius.

only the side chain of Tyr 20. The cavity disappears if the aromatic ring is rotated by ~30°. The ^{1}H NMR signals from both sides of the ring are degenerate[23] indicating that ring rotation occurs on a sub-millisecond time scale. Cavity III is thus omitted from the following discussion.

NMR Detection of water and gas molecules in cavities

The NMR detection of individual water or gas molecules in protein cavities or at specific surface sites is based on the magnetization transfer that spontaneously occurs between the protons of the water or gas molecules and the protons of the protein because of magnetic dipole-dipole interactions. Intermolecular NOEs are observed only for proton-proton distances shorter than ~3–4 Å, ensuring that the NOEs report solely on close contacts. Since bound and free water molecules exchange rapidly on the chemical shift time scale (milliseconds), only an average ^{1}H NMR signal can be resolved for the water protons[24]. Similarly, bound and free gas molecules seem to exchange rapidly. The intermolecular ligand–protein NOEs with all binding sites are thus observed in a single cross-section through 2D NOESY[25] or ROESY[26] spectra taken at the ^{1}H NMR frequency of the averaged ligand signal[27]. NOEs with protein protons separated by more than 4 Å in the three-dimensional protein structure indicate the presence of more than one ligand binding site[27,28].

NOESY and ROESY experiments detect the exchange of, respectively, longitudinal and transverse magnetization arising from NOEs. Plotting the diagonal peaks in both experiments with positive sign, an NOE between two protein protons is manifested by positive NOESY cross-peaks and negative ROESY cross-peaks. (Note that by convention, negative NOEs lead to positive NOESY and ROESY cross-peaks and *vice versa*. This article always refers to the sign of the cross-peaks.)

NOESY and ROESY spectra provide complementary information about the exchange of magnetization between ^{1}H NMR signals. First, the sign of a ROESY cross-peak is unaffected if the two interacting protons change their relative position rapidly. In contrast, NOESY cross-peaks become negative if the internuclear vector between protein and ligand protons is modulated by rapid chemical exchange of the ligand. The sign change occurs only if the motions are of large amplitude and occur within a few hundred picoseconds, that is, much faster than the overall tumbling of the protein (~10 ns at 15° C)[29]. Conversely, the observation of ROESY cross-peaks, which are not much more intense and of opposite sign than the corresponding NOESY cross-peaks, indicates that the NOE intensities are unaffected by chemical exchange between bound and free ligand[28,29]. Second, in the special case of detecting hydration water by water–protein

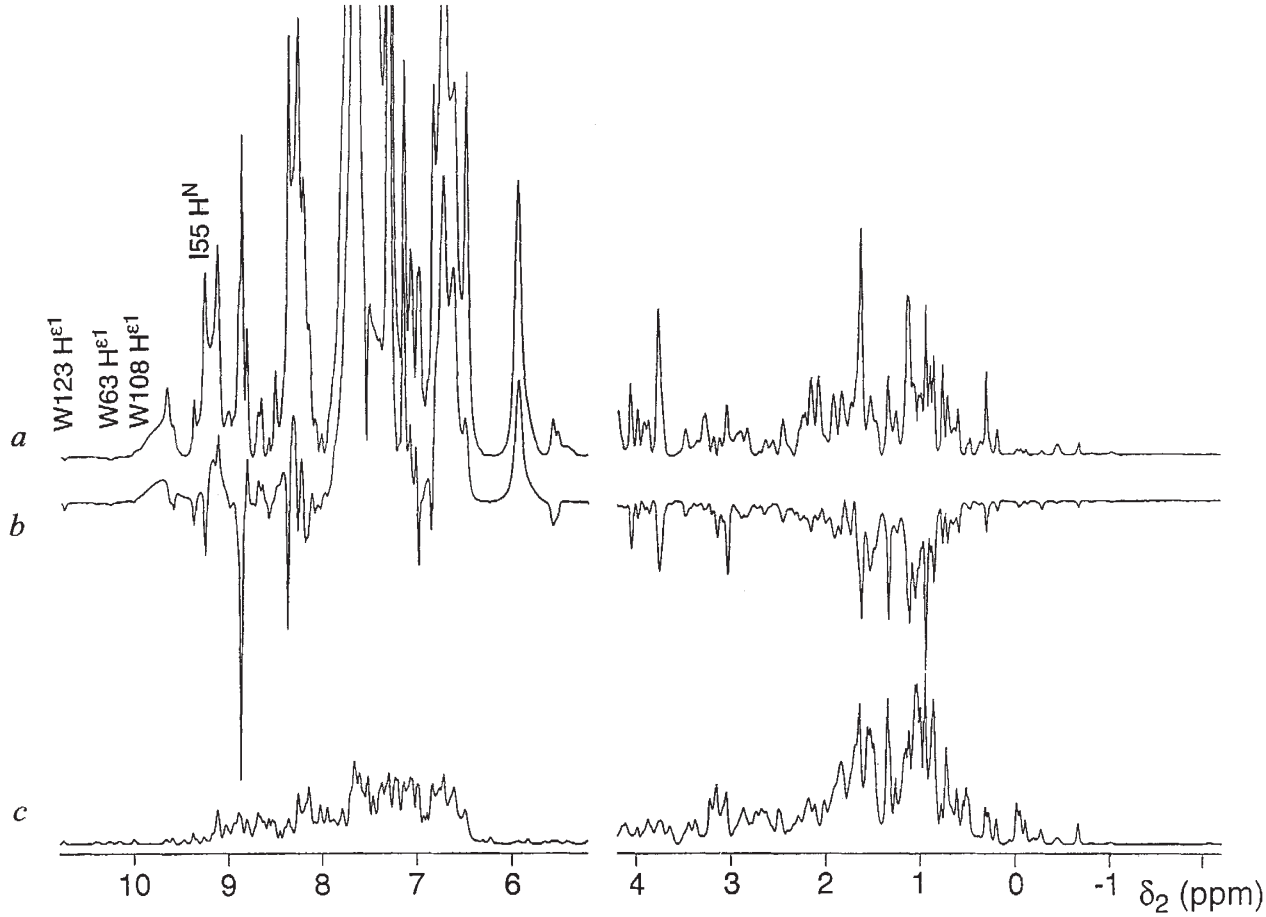

Fig. 2 Water–protein cross-peaks in NOESY and ROESY spectra of HEWL and comparison with the one-dimensional ^{1}H NMR spectrum in aqueous solutions of HEWL at pH 3.8, 36 °C. *a*, Cross-section through the NOESY spectrum. *b*, Corresponding cross-section through the ROESY spectrum. *c*, One-dimensional ^{1}H NMR spectrum. Selected water-protein NOE peaks are identified with the assignments of the protein signals involved (see text).

NOEs, NOESY and ROESY cross-peaks are also observed at the water signal when (i) protein protons exchange with the water or (ii) NOEs between non-exchangeable and exchangeable protein protons are relayed to the water signal by proton exchange with the water. Exchange peaks can be identified by their positive sign in ROESY experiments, while exchange-relayed NOEs always have the same sign as the direct NOEs. Thus, only the three-dimensional structure can tell whether a water–protein cross-peak can arise from an exchange-relayed NOE or not[28].

Detection of cavity water in HEWL

1D cross-sections taken through two-dimensional NOESY and ROESY spectra at the ^{1}H frequency of the water signal are shown in Fig. 2. The most intense cross-peaks are from direct chemical exchange between water protons and exchangeable HEWL protons. These peaks are positive in the ROESY cross-section (Fig. 2*a*,*b*)[27].

Several of the protons lining the hydrophobic cavities I and II of HEWL give rise to weak positive NOESY cross-peaks with the water signal (Figs 2,3). Their intensities are approximately one order of magnitude smaller than the NOEs typically observed with classical hydration sites, where the buried water molecules are stabilized by several hydrogen bonds to polar groups of the protein (compare to the NOE with Ile 55 HN which is hydrogen bonded to the internal water molecule W180[15]; Fig. 2). Because of their weak intensities and the spectral overlap, not all NOEs to the cavity protons could be identified. Thus, the NOE to Met 105 CεH$_3$ is the only water–HEWL NOE which could be identified for cavity II. Yet, these NOEs seem to arise unambiguously from water in cavities I and II. They cannot be explained as NOEs with protein protons at the water chemical shift. The nearest exchangeable protein or water proton to Met 105 CεH$_3$ is at a distance of ~6.8 Å (Tyr 23 Hη). Similarly, the protons of Leu 8 Cδ1H$_3$ and Leu 17 Cδ1H$_3$ of cavity I are more than, respectively, 6.5 and 5.5 Å from any proton in rapid exchange with the water. Equally intense intramolecular NOEs with the same protons correspond to distances of at most 4.5 Å. This indicates that cavities I and II are populated by water, but the weak NOE intensities suggest only partial occupancy. In particular, the NOEs are not weakened by short residence times of the water molecules, since the ROESY cross-peaks are not much more intense than the NOESY cross-peaks. This holds also for mixing times much shorter than those used for the spectra of Fig. 2 (data not shown).

Detection of gas molecules in HEWL

If they are mostly empty, hydrophobic cavities in the interior of a protein structure may be expected to bind small organic gas molecules better than water. Figs 4 and 5 show that for a variety of gases, intermolecular NOEs are indeed observed between the protons of the gas molecules and the protons lining cavities I and II in HEWL. As with water, only a single average signal was

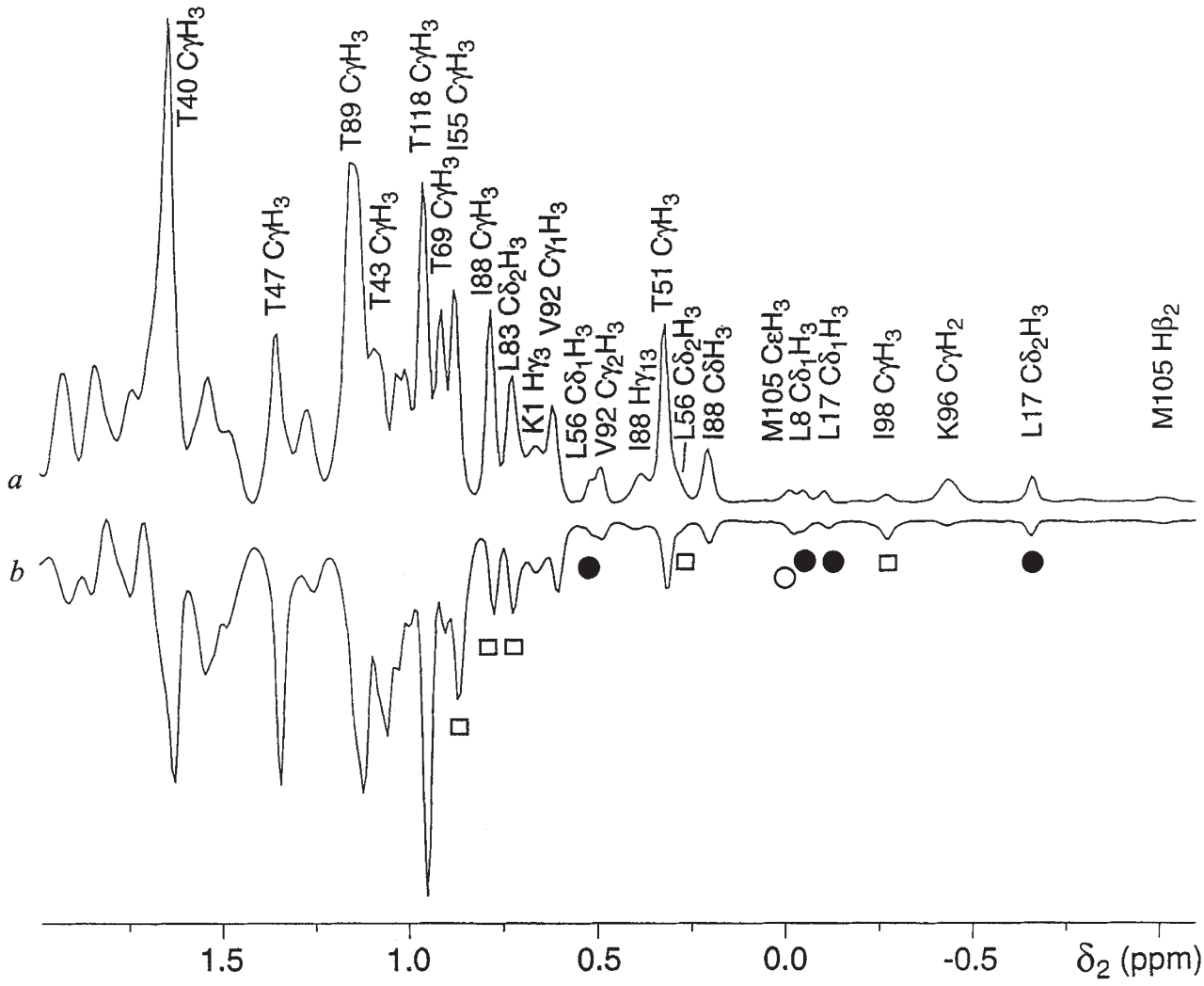

Fig. 3 Spectral region between –1 and 2 p.p.m. of the spectra of Fig. 2*a,b* with the assignments of resolved water–protein NOE peaks and exchange-relayed NOE peaks. Direct NOEs with hydration water are identified by circles and squares. The HEWL protons involved in these NOEs are more than 4.5 Å from any exchangeable water or protein proton in the crystal structure of HEWL. Squares identify NOEs with protons which are <4 Å from the oxygens of buried or mostly buried hydration water molecules which are reproducibly observed in the single crystal structures of HEWL. Filled and open circles identify NOEs with hydration water in the hydrophobic cavity I and II, respectively, which is not observed in the single crystal structures. All other assigned peaks most likely arise from exchange-relayed NOEs, since they are with protons located near exchangeable hydroxyl and amino protons of HEWL. *a*, NOESY cross-section. *b*, ROESY cross-section.

observed for each of the dissolved gases with no apparent exchange broadening. This indicates either that the gas molecules accidentally have the same chemical shifts in the cavities and in the bulk solvent, or, more likely, that they exchange within milliseconds between the two environments. Therefore, all intermolecular gas–HEWL NOEs are observed in single cross-sections through the NOESY spectra recorded with the respective gases. Methane binds with high selectivity to cavities I and II. Ethylene and cyclopropane show additional NOEs with the substrate binding site C on the surface of HEWL.

For all gases used, the intensities of the intermolecular NOEs increase with increasing pressure showing that the cavities are only incompletely populated by gas molecules even at elevated gas pressures. Larger molecules gave more intense NOEs at lower pressures (Figs 4, 5). For cyclopropane, intermolecular NOEs with HEWL could be observed even at a cyclopropane pressure of 1 bar. At 1 bar, the NOEs with site C were reduced relative to those with cavities I and II (data not shown).

Although molecular hydrogen is a much smaller molecule than, for example, methane, there is no evidence for binding to additional, smaller cavities than cavities I and II. Even at 200 bar hydrogen pressure the same NOEs are observed as with methane at 170 bar, albeit with about eight-fold reduced NOE intensities (Fig. 5).

Occupancies of cavities I and II

Up to the maximum methane pressure used (~170 bar), the intensities of the methane–HEWL NOEs increase linearly with methane concentration. Therefore, the methane occupancy can be at most 50% at 170 bar.

The intensity of the NOE between the proton of a gas molecule and a protein proton depends on the interproton distance, the overall rotational tumbling rate of the protein and the population at the gas binding site. In principle, the intermolecular NOEs also depend on the modulation of the interproton distances by very rapid exchange in and out of the binding site and

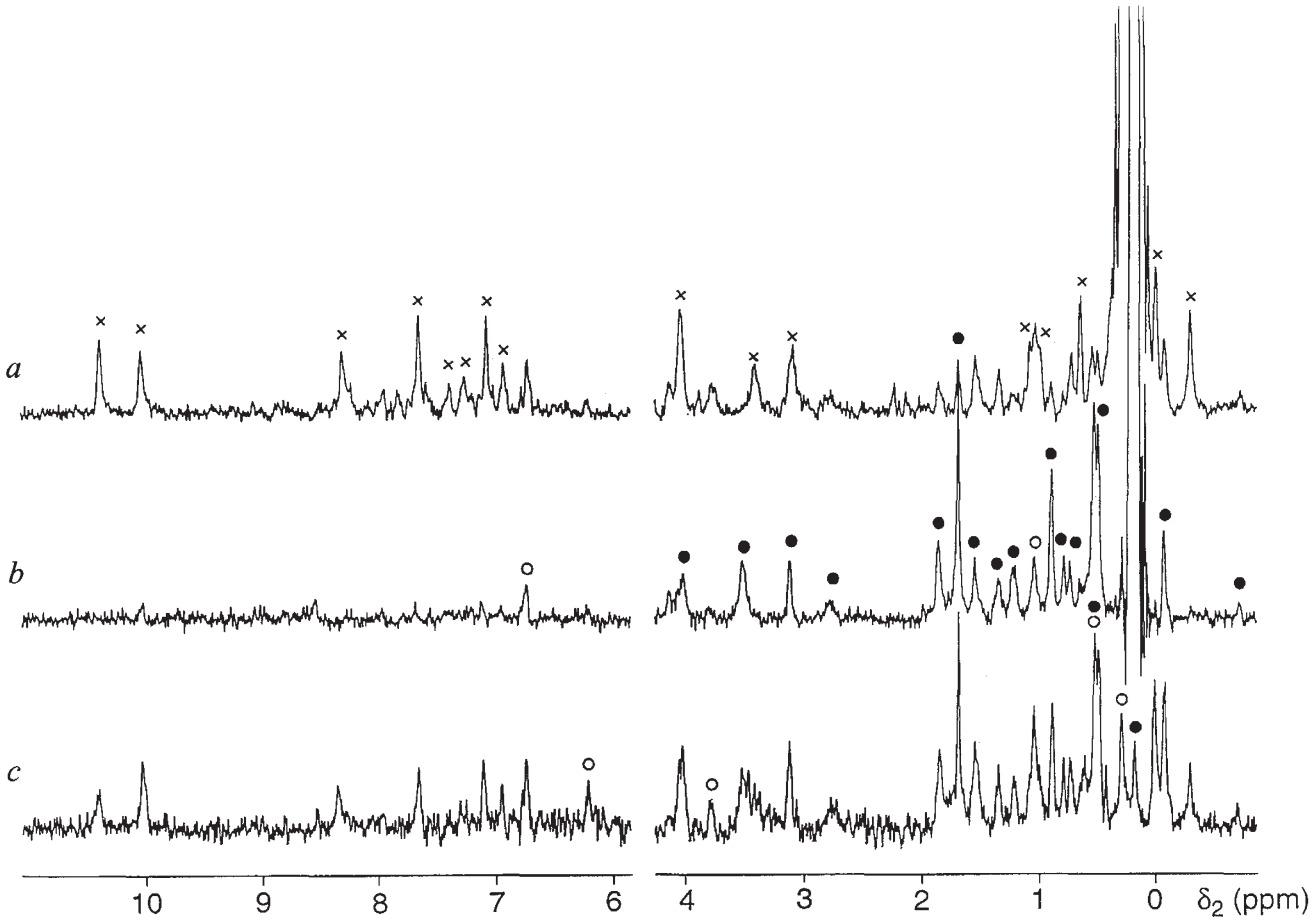

Fig. 4 Intermolecular NOEs between ethylene, methane, cyclopropane and HEWL in aqueous solution at pH 3.8, 15 °C. The spectra are cross-sections through the diagonal peaks of the respective gases in 2D NOESY spectra recorded with a spin-echo delay to suppress intra-molecular protein NOEs (see Methods). The resonance frequencies of the protein are the same in all cross-sections. Each cross-peak is identified in only one of the three cross-sections. Filled circles: NOEs with protons of cavity I. The assignments are (from left to right, ambiguous assignments in brackets): (Ser 91 Hβ2), (Ser 91 Hβ3), (Val 92 Hα), (Met 12 CγH_2), Ile 88 Hβ, Met 12 CεH_3, (Ile 55 Hγ13), Ala 32 CβH_3, (Leu 56 Hγ), Ile 55 CγH_3, Ile 88 CγH_3, (Leu 17 Hγ), Leu 56 Cδ1H_3, Val 92 Cγ2H_3, Ile 88 CδH_3, Leu 8 Cδ1H_3/Leu 17 Cδ1H_3, Leu 17 Cδ2H_3. Open circles: NOEs with cavity II. Assignments (from left to right): Trp 28 Hε3, Trp 28 Hζ3, (Trp 28 Hα), Ala 31 CβH_3, Leu 56 Cδ1H_3, (Leu 56 Cδ2H_3). Crosses: NOEs with site C. Assignments (from left to right): Trp 63 Hε1, Trp 108 Hε1, Asn 59 HN, Trp 63 Hδ1, Trp 108 Hε3, Trp 63 Hζ2, Trp 108 Hδ1, Trp 108 Hζ2, Ile 58 Hα, Asn 59 Hβ2, Asn 59 Hβ3, (Ile 58 CγH_3), (Ile 58 CδH_3), Ala 107 CβH_3, Ile 98 CδH_3, Ile 98 CγH_3. (A) Ethylene-HEWL NOEs, 450 mM ethylene at a pressure of ~80 bar. *b*, Methane-HEWL NOEs, 350 mM methane at a pressure of ~170 bar. *c*, Cyclopropane-HEWL NOEs, 180 mM cyclopropane at a pressure of ~5 bar.

by local motions of the buried gas molecule at the binding site[25,29]. As in the case of water–HEWL NOEs, however, the ROESY cross-peaks are not much more intense than the NOESY cross-peaks, even for the smallest gas molecules used (Fig. 5). Consequently, the NOEs are apparently not affected by short residence times of the gas molecules. Furthermore, it can be shown that the NOE between a protein proton and a proton of a molecule that rapidly and isotropically reorients inside a cavity is the same as the NOE with a hypothetical proton fixed at the centre of the reorienting molecule (see Box). This result has two important consequences. First, the effective NOE distance is to the centre of the cavity, that is, ~3.5 Å for most protons lining cavity I, independent of the size of the freely rotating molecule. This explains why hydrogen does not show more intense NOEs with cavity II than with cavity I compared to methane (Fig. 5), although the smaller size of cavity II favours contacts with the smaller hydrogen molecule. Second, the local reorientation rate of a trapped gas molecule does not affect the intensities of the intermolecular NOEs, as long as the rate is much faster than the overall tumbling rate of the protein. This condition certainly holds for methane and hydrogen molecules in hydrophobic cavities, since even chemically bound methyl groups in proteins rotate about their axis of symmetry with correlation times of about 50 ps or less[30]. Experimental evidence for fast methane and hydrogen reorientation is provided by the spectra shown in Fig. 5, where the ratios of the NOE intensities between the NOESY and ROESY cross-sections are, within experimental accuracy, the same in the methane–HEWL as in the hydrogen-HEWL NOE experiments. If the protein environment slowed down the reorientation rates of the trapped molecules to the 0.1–1 ns time range, the cross-peaks would be expected to be significantly larger in the ROESY than in the NOESY spectra[28] and different effects would be expected for gas molecules of different size. Given the independence from size and local reorientation rates of the trapped gas molecules in the limit of rapid isotropic reorientation, the intensities of the gas–protein NOEs depend on the effective inter-proton distance and the overall rotational tumbling rate of the protein in the same way as intra-protein NOEs. In addition, they depend on the occupancy of the cavities.

The intensities of the methane–HEWL NOEs at 170 bar methane pressure are of the same order of magnitude as NOEs

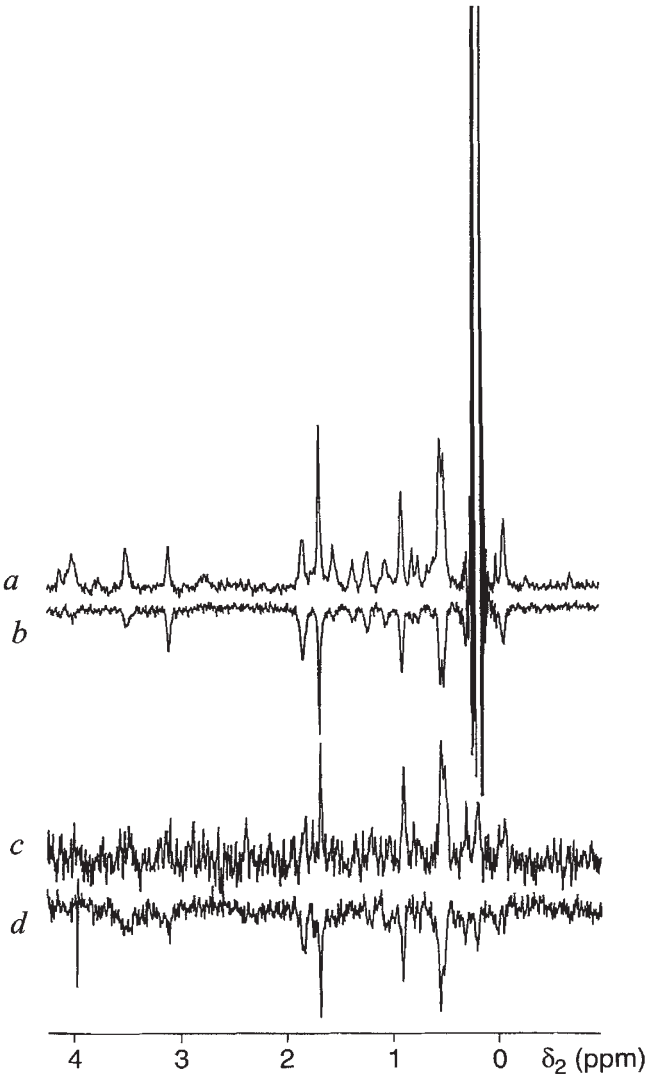

Fig. 5 Comparison between the intermolecular methane–HEWL and hydrogen–HEWL NOEs in NOESY and ROESY cross-sections at 15 °C, pH 3.8. *a*, NOESY cross-section with CH_4 (as in Fig. 4*b*). *b*, ROESY cross-section with CH_4. *c*, NOESY cross-section with H_2. 275 mM H_2 at a pressure of ~200 bar. *d*, ROESY cross-section with H_2. All spectra were scaled for equal intensity of the diagonal peaks of the dissolved gases (not plotted).

between CH_3 groups of HEWL separated by 3.5 Å. Thus, by a conservative estimate, methane populates cavity I with at least 10% and at most 50% occupancy under these conditions. The occupancies in cavity II are estimated to be about four times lower than in cavity I, based on the less intense NOEs observed, in spite of a ~1 Å smaller cavity radius (Fig. 4). Considering that methane contains twice as many protons as hydrogen, the eight-fold weaker NOEs observed with hydrogen (Fig. 5) indicate a four-fold lower occupancy compared to methane, corresponding to a difference in binding free energy of ~1 kcal mol^{-1}. An eight-fold difference in occupancy would be expected from the different solubilities of methane and hydrogen in liquid hexane[31].

At 170 bar, the intensities of the overlapping methane–Leu 56 $C\delta1H_3$/Val 92 $C\gamma2H_3$ NOEs are similar to the intensities of the corresponding NOEs with water. If the NOE transfer is twice as efficient between methane and HEWL as between water and HEWL (because there are twice as many protons in methane than in water), equal cross-peak intensities would indicate a water occupancy of at least 20% and at most 66%. The actual limits are somewhat lower, since the water–HEWL NOEs of Leu 56 $C\delta1H_3$ and Val 92 $C\gamma2H_3$ may have small contributions from NOEs with the exchangeable protons of an internal water molecule (W145[15]) and His 15 at 4.5 and 4.2 Å distance respectively.

Residence times of molecules in cavities I and II

An upper limit of 20 ms for the residence time is set by the observation that only single, averaged ^1H NMR signals can be observed for the gases in the aqueous lysozyme solution[24]. A lower limit of 1 ns is set by the positive sign observed for the intermolecular NOESY cross-peaks[28].

The positive sign of the NOESY cross-peaks provides experimental confirmation of earlier model calculations predicting that negative intermolecular water–protein NOESY cross-peaks do not come about by local reorientational motions of bound water molecules, but are manifestations of rapid translational diffusion of the water with respect to the protein surface[29].

We note that residence times >1 ns correspond to much slower diffusion rates than predicted from fluorescence quenching experiments. Using molecular oxygen to quench the fluorescence of tryptophan, it was concluded that oxygen diffuses through the protein matrix with 20–50% of its diffusion rate in water[32,33]. If hydrogen diffused through the protein with 20% of its diffusion coefficient in water ($D \approx 1X10^{-8}$ m^2 s^{-1} at room temperature[34]), the mean residence time governing the NOE would be $\tau = r^2/(6D) \approx 10$ ps for $r = 4$ Å (the distance beyond which the NOE cannot be detected). Since our lower bound on τ is two orders of magnitude larger than this, our data on HEWL are not consistent with the common view of relatively unhindered gas diffusion through proteins.

Practical aspects of gas–protein NOE measurements

Methane is an excellent NMR probe for the detection of internal hydrophobic cavities in protein structures. Its van der Waals radius is comparable to that of xenon (~2.0 Å) but it carries four protons that give rise to a single resonance in the ^1H NMR spectrum. Methane molecules can thus readily be located in a protein structure using intermolecular ^1H-^1H NOEs. Experimentally, methane was found to combine high sensitivity of detection with high specificity for the internal hydrophobic cavities I and II in HEWL.

If a cavity is initially empty and not hydrated, a population of methane molecules can be reliably detected by NOE measurements even in the absence of attractive binding forces. The density of an ideal gas at 1 bar pressure is 0.001 molecules per 40 $Å^3$, the size of cavity I in HEWL. A proportionally higher population amounting to ~20% occupancy would be expected at 200 bar. This pressure is easily achieved using sapphire NMR tubes without any modification to the NMR spectrometer[35], and occupancies as low as 1% may well be detectable by intermolecular NOEs due to the high signal intensity of the narrow methane resonance.

The ^1H NMR signals of dissolved ethylene and hydrogen are at ~5.5 and ~4.6 p.p.m. respectively, and do not interfere with the methyl resonances of a protein spectrum. However, ethylene appeared to polymerize to some degree during our experiments spoiling the protein sample.

Cyclopropane yields intermolecular NOEs of remarkable intensities at modest partial pressures. Because cyclopropane liquefies at ~5 bar, it can be used with pressure NMR tubes with-

out much danger of overpressure. Probably because it is a significantly larger probe than methane, the intermolecular NOEs with the small cavity II are weak (Fig. 4*c*). Furthermore, cyclopropane causes a broadening of the ^{1}H NMR signal of Met 12 CH_3 in cavity I which was not observed with methane, ethylene or hydrogen, perhaps because its relative bulkiness restricts the motional freedom of this side chain.

Solvation of hydrophobic cavities by organic solvents

Intermolecular NOEs with the protons lining cavities I and II in HEWL were also observed with methylene chloride at 0.2 M[9]. Population of cavity I was evidenced by NOEs with Ile 55 CγH_3 and Leu 56 Cδ1H_3 and Cδ2H_3, while the NOEs observed with Ala 31 CβH_3, Leu 56 Cδ2H_3, and Met 105 CεH_3 indicate population of cavity II. Further intermolecular NOEs to the cavity protons probably occur but are difficult to identify because of spectral overlap. Like larger organic solvent molecules, methylene chloride primarily binds to the substrate binding site C[9].

Solvation of the substrate binding site C

Among six consecutive binding sites in the active site cleft of HEWL, site C has the highest affinity for the natural substrate of HEWL and has been shown to bind a large variety of small organic solvent molecules[9]. Like organic solvents, cyclopropane and ethylene show intense NOEs with Trp 63 Hε1, Trp 108 Hε1 and Ile 98 CδH_3 (Fig. 4). In contrast, only weak water–HEWL NOEs were observed with these protons. The negative signs of the NOESY cross-peaks with Trp 63 Hε1 (Fig. 2) and Ile 98 CδH_3 (from NOE-NOESY experiments, data not shown) indicate water residence times of <0.5 ns[28,29]. The NOESY cross-peak between water and Trp 108 Hε1 is positive (Fig. 2), but it is weaker than expected for a stable hydration shell with high occupancy. Since site C is filled with water molecules with >85% occupancy in the crystal structures of HEWL[11–20], the water–Trp 108 Hε1 NOE appears to be weakened by short water residence times of at most a few nanoseconds. Clearly, the unstable hydration of site C favours the binding of hydrophobic molecules like ethylene and cyclopropane.

Binding specificity of small organic molecules

The origin of the observed selectivity of gases and organic solvents for empty hydrophobic cavities can be explained by the energetic cost to replace a polar water molecule by a nonpolar gas molecule of similar size. The interaction energy required to populate a cavity with water with near 100% occupancy has been estimated to be below –12 kcal mol^{-1}, a value comparable to the interaction energy in ice[4]. This much stabilization energy necessitates the formation of hydrogen bonds or equivalent, strong electrostatic interactions. If hydrogen bonding contributed as little as –2 kcal mol^{-1} to the stabilization of a cavity water molecule, its replacement by a nonpolar molecule of similar size would be disadvantaged by ~30-fold compared to the situation where the cavity is empty from the beginning. In a larger cavity, several water molecules can form hydrogen bonds to one another, decreasing the energetic penalty for the transfer from the bulk water to the cavity. In this situation, a cluster of mutually hydrogen-bonded water molecules may be present even if the cavity is hydrophobic and does not favour polar molecules over non-polar molecules. In contrast to a single water molecule in a polar cavity, a water cluster in a hydrophobic environment would presumably provide less hindrance to the entry of a nonpolar ligand which is able to replace all water molecules of the cluster simultaneously by matching the shape of the binding site. It has been shown for cavity forming mutants of T4 lysozyme that larger cavities favour the binding of larger ligands[36].

Small molecules with anesthetic properties are invariably hydrophobic. It has been shown that cyclopropane and similar compounds with anesthetic properties are highly soluble in fat and lipids[37] and also bind to hydrophobic protein cavities[6,7,38,39]. Proteins are probably involved in the anesthetic effect, because anesthetic resistant mice can be bred[40]. The present study shows that the prime binding sites of organic gas and solvent molecules are devoid of water. Binding to hydrated sites like site C in HEWL is possible, if hydration of the site is unstable. Binding to empty or nearly empty hydrophobic cavities in proteins or at interfaces between proteins and other biological structures like membranes is the first effect that must be expected when proteins are exposed to organic gas molecules. Such binding may impair protein function sufficiently to cause anesthesia.

Methods

Solution structure of HEWL and resonance assignments. The hydrophobic core of HEWL in solution is indistinguishable from that in the X-ray crystal structures[41]. By comparing the NOEs expected from the crystal structure with the observed NOEs, we stereospecifically assigned the ^{1}H resonances involved in intermolecular NOEs with water or gas molecules. The assignments obtained in this way were in full agreement with the ring current shifts predicted from the crystal structure coordinates.

Algorithm for the identification of cavity space. The cavity space in the crystal structure of HEWL was determined by a grid search algorithm. A three-dimensional grid was superimposed onto the structure coordinates with 0.5 Å grid point separation. Grid points, where spheres of 0.5 Å radius could be accommodated without van der Waals violations with protein atoms, were selected. The selected grid points were checked for whether they could also accommodate spheres of 1.4 Å radius. If van der Waals violations were detected, the grid point was shifted by up to 0.5 Å in all three dimensions in steps of 0.1 Å to search for a location without van der Waals violations. If no location without van der Waals violations was found, the grid point was dropped from the selection. If two grid points ended up within 0.1 Å of one another, one of them was dropped. The outer surface of the protein was defined by a separate grid search performed with 0.5 Å grid point separation and a spherical probe of 1.4 Å radius. Prior to the grid searches, the heavy atoms of the crystal coordinates (2LYM[15]) were supplemented by hydrogens using standard bond angles and bond lengths. Van der Waals radii used for the grid search were 1.5 Å for C, 1.35 Å for O, 1.45 Å for N, 1.7 Å for S and 1.0 Å for H. The algorithm computes similar cavity volumes as that of Connolly[42], except that because of the smaller radii used here, smaller cavities were detected and somewhat larger volumes ascribed to them. Fig. 1 was generated using MolScript[43].

NMR recordings at 200 bar. The NMR spectra were recorded with 11 mM solutions of hen egg-white lysozyme (Fluka AG, Switzerland) in 90% ^1H_2O/10% ^2H_2O at pH 3.8 and a ^{1}H frequency of 600 MHz on a Bruker DMX 600 NMR spectrometer. Experiments at elevated gas pressure ≤ 200 bar were performed using a sapphire NMR tube of 5 mm outer diameter and 3.4 mm inner diameter fitted with a titanium valve[35].

Measurement of water-HEWL NOEs. 2D NOESY and ROESY experiments for the detection of water–HEWL NOEs were recorded using the sequence τ–SL before detection for water suppression, where τ was 100 µs, the duration of the spin-lock pulse SL was 1 ms, and the carrier frequency was at the water reso-

nance[24,44]. The water suppression in the NOESY spectra was improved by homospoil pulses during the mixing time. The use of a spin-lock pulse for water suppression resulted in an excitation profile along the F_2 frequency axis described by $\sin(2\pi\nu\tau)$, where ν is the offset from the carrier frequency in Hz. For improved readability, the spectral region between 5 and 11 p.p.m. in Fig. 2 was inverted to compensate for the sign inversion caused by the excitation profile. The spectra of Fig. 2 were recorded using t_{1max}=52 ms, t_{2max}=118 ms, 50 ms mixing time, and recording times of 13 h.

Because of the extensive spectral overlap in the 1D NOESY and ROESY spectra, most of the cross-peaks were assigned from 2D NOE-NOESY, NOE-TOCSY, ROE-NOESY and ROE-TOCSY experiments, in which the water signal was selectively excited and the NOEs with the protein resolved by cross-peaks with further protein protons[45,46]. Cross-peaks were identified as water–HEWL NOEs only, if the protein protons were at least 4 Å from any rapidly exchanging proton of hydroxyl, amino, guanidinium and imidazol groups in the three-dimensional structure of HEWL.

Measurement of gas-HEWL NOEs. NOESY and ROESY spectra for the selective observation of intermolecular gas–HEWL NOEs were recorded by replacing the initial 90° pulse of the conventional pulse sequences by the sequence 90°–HS–Δ–180°(selective)–HS–Δ^9, where HS denote homospoil spoil pulses of 2 ms duration applied with a sine shaped amplitude. The delay Δ was set to 100 ms. The 180°(selective) pulse was a 10 ms RE-BURP pulse[47] at the frequency of the ^{1}H resonance of the dissolved gas. The spin-echo sequence effectively filters the signal of the small gas molecules by two effects: (i) only the magnetization refocused by the selective 180° pulse is also refocused by the second homospoil pulse magnetization; (ii) the ^{1}H magnetization of HEWL relaxes virtually completely during 200 ms of transverse relaxation. The spectra of Figs 4 and 5 were recorded with the following parameters: t_{1max}=100 ms, t_{2max}=223 ms, mixing time 100 ms in NOESY and 50 ms in ROESY experiments, total recording time=16 h per spectrum. The water signal was suppressed by selective pre-irradiation. No significant NOE enhancement was observed between the ^{1}H NMR signals of the dissolved gases and the water. The intermolecular NOEs were assigned by comparison with conventional NOESY and TOCSY[48] experiments recorded under the same conditions. The concentrations of the dissolved gases were determined by integration of their ^{1}H NMR signal and comparison with the intensities of resolved resonances of HEWL.

Acknowledgments

Financial support from the Swedish Natural Science Research Council is gratefully acknowledged.

Received 10 December 1996; Accepted 14 March 1997

Box 1 Effect of fast internal motion on intermolecular NOEs

The cross-relaxation rates responsible for cross-peaks in NOESY and ROESY spectra are governed by the spectral density, $j(\omega)$, of the magnetic dipole coupling at multiples of the Larmor frequency ω_0 [25]. For an isotropically tumbling protein (correlation time τ_R) with a fast internal motion (correlation time τ_I, with $\tau_I << \tau_R$, $1/\omega_0$)[49,50],

$$(1) \qquad j(\omega) = A^2 \frac{\tau_R}{1 + (\omega\tau_R)^2} \; [\langle R^{-6}\rangle - A^2]\tau_I$$

with the generalized order parameter

$$(2) \qquad A^2 = \sum_{q=-2}^{2} |\langle F_{2q}(\mathbf{R})\rangle|^2$$

involving the solid spherical harmonics $F_{kq}(\mathbf{R})=C_{kq}(\Omega)/R^{k+1}$ of rank k=2. Here $\mathbf{R}$ is the interproton vector, of length R and orientation $\Omega=(\theta,\phi)$, the $C_{kq}(\Omega)$ are (unnormalized) sperical harmonics, and $\langle ... \rangle$ represents an average over the equilibrium distribution of $\mathbf{R}$ associated with the internal degree(s) of freedom. In the absence of internal motion (fixed $\mathbf{R}$), $A^2=R^{-6}$.

The generalized order parameter is most conveniantly evaluated in a coordinate system with origin at the centre of symmetry of the internal motion rather than at the proton. If only one of the two coupled protons undergoes internal motion, the solid harmonics can be transformed to the centre of symmetry according to[51]

$$(3) \qquad \langle F_{2q}(\mathbf{R})\rangle = \sum_{k=2}^{\infty} R_1^{k-2} \sum_{p=-k}^{k} B_{kpq} \langle C_{k-2,q-p}(\Omega_1)\rangle F_{kp}(\mathbf{R}_2)$$

where $\mathbf{R}_1=(R_1,\Omega_1)$ and $\mathbf{R}_2=(R_2,\Omega_2)$ are vectors from the center of symmetry to the mobile and fixed proton, respectively, and $R_1<R_2$ is assumed. Further, $B_{kpq}=(-1)^{p+q}\{(k-p)!(k+p)!/[(2-q)!(2+q)!(k-2-p+q)!(k-2+p-q)!]\}^{1/2}$.

If the mobile-proton vector $\mathbf{R}_1$ is distributed with spherical symmetry, it follows from the orthogonality of the spherical harmonics that $\langle C_{k-2,q-p}(\Omega_1)\rangle = \delta_{k2}\delta_{qp}$, whereby $\langle F_{2q}(\mathbf{R})\rangle = F_{2q}(\mathbf{R}_2)$. Inserting this into equation 2 and using the closure relation for spherical harmonics, we obtain $A^2=R_2^{-6}$, that is, the same result as if the spherically disordered proton were fixed at the center of symmetry. For internal motion of lower symmetry, corrections to this result appear that are proportional to an internal order parameter S_{int} and a power of $z=R_1/R_2$. As $S_{int}<<1$ for an orientationally disorderd ligand molecule and $R_1/R_2<1$, these corrections are small. By employing a two-centre expansion for solid harmonics[51], internal motions of both protons can be handled in a similar way. When both protons are spherically disordered, A^2 is the same as if they were located at the centres of symmetry.

To calculate the spectral density in equation 1, we also need the average $\langle R^{-6}\rangle$. This is most conveniantly obtained from a Laplace-type expansion[52] of R^{-6}. For a spherically disordered proton, we thus obtain $\langle R^{-6}\rangle = R_2^{-6}(1+z^2)/(1-z^2)^4$. With R_1=1 Å and R_2=3.5 Å, as appropriate for methane in cavity I, the relative weight of the second term in equation 1, that is $\langle R^{-6}\rangle/A^2-1$, is 0.52. (Alternatively, if the order parameter is defined as $S=A/\langle R^{-6}\rangle^{1/2}$, then S=0.81) A simple calculation then shows that the second term in equation 1, which depends on the rate of the internal motion, makes a negligible (<3% if τ_R=10 ns) contribution to the NOESY and ROESY cross-peak intensities at 600 MHz as long as τ_I <0.1 ns.

1. Ernst, J.A., Clubb, R.T., Zhou, H.X., Gronenborn, A.M. & Clore, G.M. Demonstration of positionally disordered water within a protein hydrophobic cavity by NMR. *Science* **267**, 1813–1817 (1995).
2. Matthews, B.W., Morton, A.G. & Dahlquist, F.W. Use of NMR to detect water within nonpolar protein cavities. *Science* **270**, 1847–1848 (1995).
3. Ernst, J.A., Clubb, R.T., Zhou, H.X., Gronenborn, A.M. & Clore, G.M. Use of NMR to detect water within nonpolar protein cavities – response. *Science* **270**, 1848–1849 (1995).
4. Zhang, L. & Hermans, J. Hydrophilicity of cavities in proteins. *Proteins* **24**, 433–438 (1996).
5. Buckle, A.M., Cramer, P. & Fersht, A.R. Structural and energetic responses to cavity-creating mutations in hydrophobic cores: observation of a buried water molecule and the hydrophilic nature of such hydrophobic cavities. *Biochemistry* **35**, 4298–4305 (1996).
6. Schoenborn, B.P,. Watson, H.C. & Kendrew, J.C. Binding of xenon to sperm whale myoglobin. *Nature* **207**, 28–30 (1965).
7. Schoenborn, B. P. Binding of cyclopropane to sperm whale myoglobin. *Nature* **214**, 1120–1122 (1967).
8. Shulman, R.G., Peisach, J. & Wyluda, B.J. Effects of cyclopropane and xenon upon the high-resolution nuclear magnetic resonance spectrum of ferrimyoglobin cyanide. *J. Mol. Biol.* **48**, 517–523 (1970).
9. Liepinsh, E. & Otting, G. Organic solvents identify specific ligand binding sites on protein surfaces. *Nature Biotech.*, **5**, 264–268 (1997).
10. Bernstein, F.C., Koetzle, T.F., Williams, G.J.B., Meyer Jr., E.F., Brice, M.D., Rodgers, J.R., Kennard, O., Shimanouchi, T. & Tasumi, M. The protein data bank: a computer-based archival file for macromolecular structures. *J. Mol. Biol.* **112**, 535–542 (1977).
11. Kodandapani, R. Suresh, C.G. & Vijayan, M. Crystal structure of low humidity tetragonal lysozyme at 2.1 Å resolution. Variability in hydration shell and its structural consequences. *J. Biol. Chem.* **265**, 16126–16131 (1990).
12. Wilson, K.P., Malcolm, B.A. & Matthews, B.W. Structural and thermodynamic analysis of compensating mutations within the core of chicken egg white

lysozyme. *J. Biol. Chem.* **267**, 10842–10849 (1992).
13. Hodsdon, J.M., Brown, G.M., Sieker, L.C. & Jensen, L.H. Refinement of triclinic lysozyme: I. Fourier and least-squares methods. *Acta Crystallogr.* **B46**, 54–62 (1990).
14. Ramanadham, M., Sieker, L.C. & Jensen, L.H. Refinement of triclinic lysozyme: II. the method of stereochemically restrained least squares. *Acta Crystallogr.* **B46**, 63–69 (1990).
15. Kundrot, C.E. & Richards, F.M. Crystal structure of hen egg-white lysozyme at a hydrostatic pressure of 1000 atmospheres. *J. Mol. Biol.* **193**, 157–170 (1987).
16. Young, A.C.M., Dewan, J.C., Nave, C. & Tilton, R.F. Comparison of radiation-induced decay and structure refinement from X-ray data collected from lysozyme crystals at low and ambient temperatures. *J. Appl. Crystallogr.* **26**, 309–319 (1993).
17. Lescar, J., Souchon, H. & Alzari, P.M. Crystal structure of pheasant and guinea fowl egg-white lysozymes. *Protein Sci.* **3**, 788–798 (1994).
18. Chitarra, V., Alzari, P.M., Bentley, G.A., Bhat, T.N., Eisele, J.L., Houdusse, A., Lescar, J., Souchon, H. & Poljak, R.J. Three-dimensional structure of a heteroclitic antigen-antibody cross-reaction complex. *Proc. Natl. Acad. Sci. USA* **90**, 7711–7715 (1993).
19. Shih, P., Holland, D.R. & Kirsch, J.F. Thermal stability determinants of chicken egg-white lysozyme core mutants: hydrophobicity, packing volume, and conserved buried water molecules. *Protein Sci.* **4**, 2050–2062 (1995).
20. Wilson, K.P., Malcolm, B.A. & Matthews, B.W. Structural and thermodynamic analysis of compensating mutations within the core of chicken egg white lysozyme. *J. Biol. Chem.* **267**, 10842–10849 (1992).
21. Cheetham, J.C., Artymiuk, P.J. & Phillips, D.C. Refinement of an enzyme complex with inhibitor bound at partial occupancy. Hen egg-white lysozyme and tri-N-acetylchitotriose at 1.75 angstroms resolution. *J. Mol. Biol.* **224**, 613–628 (1992).
22. Hadfield, A.T., Harvey, D.J., Archer, D.B., MacKenzie, D.A., Jeenes, D.J., Radford, S.E., Lowe, G., Dobson, C.M. & Johnson, L.N. Crystal structure of the mutant D52S hen egg white lysozyme with an oligosaccharide product. *J. Mol. Biol.* **243**, 856–872 (1994).
23. Redfield, C. & Dobson, C.M. Sequential ^{1}H NMR assignments and secondary structure of hen egg white lysozyme in solution. *Biochemistry* **27**, 122–136 (1988).
24. Otting, G., Liepinsh, E. & Wüthrich, K. Proton exchange with internal water molecules in proteins in aqueous solution. *J. Am. Chem. Soc.* **113**, 4363–4364 (1991).
25. Ernst, R.R., Bodenhausen, G. & Wokaun, A. Principles of Nuclear Magnetic Resonance in One and Two Dimensions (Clarendon Press, Oxford; 1987).
26. Bothner-By, A.A., Stephens, R.L., Lee, J., Warren, C.D. & Jeanloz, R.W. Structure determination of a tetrasaccharide: transient nuclear Overhauser effects in the rotating frame. *J. Am. Chem. Soc.* **106**, 811–813 (1984).
27. Otting, G. & Wüthrich, K. Studies of protein hydration in aqueous solution by direct NMR observation of individual protein-bound water molecules. *J. Am. Chem. Soc.* **111**, 1871–1875 (1989).
28. Otting, G. & Liepinsh, E. Protein hydration by high-resolution NMR spectroscopy - implications for MR image contrast. *Acc. Chem. Res.* **28**, 171–177 (1995).
29. Otting, G., Liepinsh, E. & Wüthrich, K. Protein hydration in aqueous solution. *Science* **254**, 974–980 (1991).
30. Lipari, G. & Szabo, A. Model-free approach to the interpretation of nuclear magnetic resonance relaxation in macromolecules. 2. Analysis of experimental results. *J. Am. Chem. Soc.* **104**, 4559–4570 (1982).
31. Fogg, P.G.T. & Gerrard, W. Solubility of Gases in Liquids (Wiley, Chichester; 1991).
32. Lakowicz, J. R. & Weber, G. Quenching of protein flourescence by oxygen. Detection of structural fluctuations in proteins on the nanosecond time scale. *Biochemistry* **12**, 4171–4179 (1973).
33. Calhoun, D.B., Vanderkooi, J.M., Woodrow III, G.V. & Englander, S.W. Penetration of dioxygen into proteins studied by quenching of phosphorescence and flourescence. *Biochemistry* **22**, 1526–1532 (1983).
34. Gmelin Handbuch der Anorganischen Chemie, 8th edition, Vol. 2, p. 111 (Verlag Chemie, Weinheim; 1926).
35. Cusanelli, A., Frey, U., Richens, D.T. & Merbach, A.E. The slowest water exchange at a homoleptic mononuclear metal center - variable-temperature and variable-pressure 17O NMR study on $[Ir(H_2O)_6]^{3+}$. *J. Am. Chem. Soc.* **118**, 5265–5271 (1996).
36. Morton, A., Baase, W.A. & Matthews, B.W. Energetic origins of specificity of ligand binding in an interior nonpolar cavity of T4 lysozyme. *Biochemistry* **34**, 8564–8575 (1995).
37. Taheri, S., Halsey, M.J., Liu, J., Eger II, E.I., Koblin, D.D. & Laster, M.J. What solvent best represents the site of action of inhaled anesthetics in humans, rats, and dogs? *Anesth. Analg.* **72**, 627–634 (1991).
38. Gursky, O., Fontano, E., Bhyravbhatla, B. & Caspar, D.L. Stereospecific dihaloalkane binding in a pH-sensitive cavity in cubic insulin crystals. *Proc. Natl. Acad. Sci. USA* **91**, 12388–12392 (1994).
39. Nakagawa, T., Hamanaka, T., Nishimura, S., Uruga, T. & Kito, Y. The specific binding site of the volatile anesthetic diiodomethane to purple membrane by X-ray diffraction. *J. Mol. Biol.* **238**, 297–301 (1994).
40. Koblin, D.D., Deady, J.E. & Eger, E.I. Potencies of inhaled anesthetics and alcohol in mice selectively bred for resistance and susceptibility to nitrous oxide anesthesia. *Anesthesiology* **56**, 18–24 (1982).
41. Smith, L.J., Sutcliffe, M.J., Redfield, C. & Dobson, C.M. Structure of hen lysozyme in solution. *J. Mol. Biol.* **229**, 930–944 (1993).
42. Connolly, M.L. Atomic size packing defects in proteins. *Int. J. Peptide Prot. Res.* 28, 360–363 (1986).
43. Kraulis, P. Molscript: a program to produce both detailed and schematic plots of protein structures. *J. Appl. Crystallogr.* **24**, 946–950 (1991).
44. Otting, G., Liepinsh, E., Farmer II, B.T. & Wüthrich, K. Protein hydration studied with homonuclear 3D ^{1}H NMR experiments. *J. Biomol. NMR* **1**, 209–215 (1991).
45. Otting, G. & Liepinsh, E. Selective excitation of the water signal by a Q-switched selective pulse. *J. Magn. Reson.* B **107**, 192–196 (1995).
46. Otting, G. & Liepinsh, E. Selective excitation of intense solvent signals in the presence of radiation damping. *J. Biomol. NMR* **5**, 420–426 (1995).
47. Geen, H. & Freeman, R. Band-selective radiofrequency pulses. *J. Magn. Reson.* **93**, 93–141 (1991).
48. Briand, J. & Ernst, R.R. Computer-optimized homonuclear TOCSY experiments with suppression of cross relaxation. *Chem. Phys. Lett.* **185**, 276–285 (1991).
49. Halle, B. & Wennerström, H. Interpretation of magnetic resonance data from water nuclei in heterogeneous systems. *J. Chem. Phys.* **75**, 1928–1943 (1981).
50. Lipari, G. & Szabo, A. Model-free approach to the interpretation of nuclear magnetic resonance relaxation in macromolecules. I. Theory and range of validity. *J. Am. Chem. Soc.* **104**, 4546–4559 (1982).
51. Chiu, Y. Irreducible tensor expansion of solid spherical harmonic-type operators in quantum mechanics. *J. Math. Phys.* **5**, 283–288 (1964).
52. Sack, R.A. Generalization of Laplace's expansion to arbitrary powers and functions of the distance between two points. *J. Math. Phys.* **5**, 245–251 (1964).